Inorganic Chemistry

Article

pubs.acs.org/IC

Next Generation PhotoCORMs: Polynuclear Tricarbonylmanganese(I)-Functionalized Polypyridyl Metallodendrimers

Preshendren Govender,[†] Sandesh Pai,[‡] Ulrich Schatzschneider,*[,‡] and Gregory S. Smith*[,†]

[†]Department of Chemistry, University of Cape Town, Rondebosch, 7701, Cape Town, South Africa

[‡]Institut für Anorganische Chemie, Julius-Maximilians-Universität Würzburg, Am Hubland, D-97074 Würzburg, Germany

Supporting Information

ABSTRACT: The first CO-releasing metallodendrimers, based on polypyridyl dendritic scaffolds functionalized with $Mn(CO)_3$ moieties, of the general formula $[DAB\text{-}PPI\text{-}\{MnBr(bpy^{CH3,CH=N})(CO)_3\}_n]$, where DAB = 1,4-diaminobutane, PPI = poly(propyleneimine), bpy = bipyridyl, and n = 4 for first- or n = 8 for second-generation dendrimers, were synthesized and comprehensively characterized by analytical (HR-ESI mass spectrometry and elemental analysis) and spectroscopic (^1H, $^{13}C\{^1H\}$-NMR, infrared, and UV/vis spectroscopy) methods. The CO-release properties of these compounds were investigated in pure buffer and using the myoglobin assay. Both metallodendrimer generations are stable in the dark in aqueous buffer for up to 16 h but show photoactivated CO release upon excitation at 410 nm, representing a novel class of macromolecular photoactivatable CO-releasing molecules (PhotoCORMs). No scaling effects were observed since both metallodendrimers release ~65% of the total number of CO ligands per molecule, regardless of the generation number. In addition, the mononuclear model complex $[MnBr(bpy^{CH3,CH=NCH2CH2CH3})(CO)_3]$ was prepared and comprehensively studied, including DFT/TDDFT calculations. These metallodendrimer-based PhotoCORMs afford new methods of targeted delivery of large amounts of carbon monoxide to cellular systems.

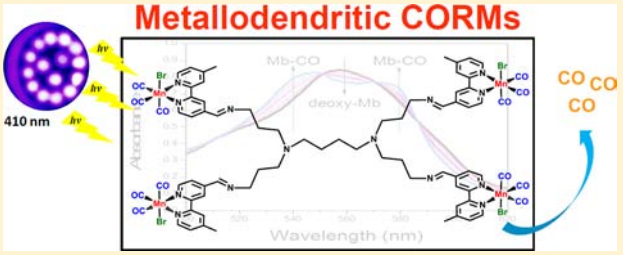

INTRODUCTION

For decades, the odorless, tasteless, and colorless gas carbon monoxide has been viewed as highly toxic to humans, due to its deleterious effects on oxygen metabolism.[1] However, small molecules such as nitric oxide and hydrogen sulfide have now been established as important, endogenously produced, signaling molecules in higher organisms, including humans.[2,3] This is also true for CO, which is one of the products of the enzymatic degradation of heme by heme oxygenase (HO), the other two being ferric iron and biliverdin, with the latter further converted to bilirubin by biliverdin reductase.[4] In addition to the important vasodilatory effects of CO, it is its cytoprotective activity, in particular against oxidative stress mediated by reactive oxygen species (ROS), that has become the focus of recent research due to potential therapeutic applications of CO outweighing its toxicity.[5] Since the tissue accumulation of CO is determined by the distribution coefficient between the different cellular environments, which is a fixed parameter, other carrier systems for CO with a "drug sphere" that can be tuned for specific medicinal applications are now actively pursued. Transition metal carbonyl complexes are a natural choice as CO-prodrugs, and a number of trigger mechanisms to initiate CO release from the metal coordination sphere have been developed for such *CO-releasing molecules* (CORMs).

Motterlini and co-workers have pioneered the development of CORMs with the use of $Mn_2(CO)_{10}$ (CORM-1)[6] and the synthesis of $[RuCl_2(CO)_3]_2$ (CORM-2),[7] which induce vasodilatation, attenuate coronary vasoconstriction, and reduce acute hypertension.[7] The poor solubility of CORM-1 and CORM-2 under physiological conditions led to the synthesis of the water-soluble complex [*fac*-RuCl(glycinate)$(CO)_3$] (CORM-3), which showed more promising results and is now the most popular compound for many biological studies.[8] However, due to the complicated speciation of CORM-3 in solution,[9] researchers directed their attention to other transition metals.[10−15] Alternative CORMs that have been explored include pyrone-substituted iron and molybdenum carbonyl complexes, which undergo solvent-assisted CO release.[16,17] More recently, Romão et al. synthesized a series of $Mo(CO)_3$-based complexes with a wide range of biomedical applications, focusing on inflammation, infection, and vasorelaxation, with a recent review detailing the requirements of CORMs for clinical applications.[18]

In addition to compounds in which the CO release is induced by ligand exchange reactions with solvent or other dissolved species, enzyme-triggered CO release (ET-CORMs)

Received: February 13, 2013
Published: April 17, 2013

   dx.doi.org/10.1021/ic400377k | *Inorg. Chem.* 2013, 52, 5470−5478

has been demonstrated by the group of Schmalz.[19−21] Another important technique is based on the light-induced CO release in PhotoCORMs developed by Ford, Schatzschneider, and others.[22−26] Light has already been used to elicit biological responses in "caged" compounds[27,28] as well as in the context of photodynamic therapy, but the latter is based on the formation of reactive singlet oxygen by photosensitizers[29,30] instead of active species with a more well-defined spectrum of cellular targets. Hence, the synthesis of light-activated water-soluble molybdenum-containing CORMs $[Mo(C{\equiv}CCR^1R^2OH)(\eta^5\text{-}C_5H_5)(CO)_3]$ (where $R^1 = R^2 = Me$ or $R^1 = Me$, $R^2 = Ph$) was pursued.[31] The photoinduced release of carbonyl ligands and the efficient cellular uptake by HT-29 human colon cancer cells of a Mn-functionalized CORM, i.e., $[Mn(CO)_3(tpm)]PF_6$ (where tpm = tris(pyrazolyl)methane),[32] prompted the investigation into the biocompatibility and the targeting ability of this novel CORM. With the use of Pd-catalyzed Sonogashira cross-coupling and "click" reactions, alkyne-functionalized $[Mn(CO)_3(tpm)]PF_6$ was conjugated to amino acids and model peptides.[33] Notably, the incorporation to the bioconjugate did not alter the CO-release properties of the metal carbonyl moiety. More recently, grafting of the substituted $[Mn(CO)_3(tpm)]^+$ moiety to silicium dioxide and carbon nanomaterials, designed to deliver CO to solid tumors, was demonstrated with photoinduced CO-release properties similar to the parent compound.[34,35] A common problem with all the reported CORMs, regardless of the trigger mechanism for CO release, however, is the fact that in addition to the CO liberated, there is always an inevitable formation of a metal-coligand fragment, which might possess biological activity of its own. One strategy to address this problem is based on systems in which the metal−ligand moiety generated after CO release remains bound to a macromolecular carrier. In addition to different polymeric materials,[36] dendrimers are an attractive choice for this purpose due to their monodisperse nature and facile preparation. Furthermore, such macromolecules are known to passively accumulate in tumor tissue due to the enhanced permeability and retention (EPR) effect.[37] Metallodendrimers are dendrimers decorated with metal-containing moieties, which have been extensively explored in the field of catalysis.[38,39] Only recently, have they also been investigated as potential therapeutic agents,[40,41] since their multifunctionality may lead to an increased interaction between a dendrimer-drug conjugate and a cellular target bearing multiple receptors. Here, we report tetranuclear and octanuclear $Mn(CO)_3$-functionalized CO-releasing metallodendrimers (**1**, **2**) based on a polypyridyl dendritic scaffold. In order to compare the scaling of the CO release of these compounds with the number of metal carbonyl end groups, a mononuclear analogue (**3**) was also synthesized as a model for the polynuclear metallodendrimers.

RESULTS AND DISCUSSION

Synthesis of Dendritic Ligands and Complexes. The dendritic ligands **L1** and **L2** were prepared *via* a Schiff-base condensation reaction of 4′-methyl-2,2′-bipyridine-4-carboxaldehyde with DAB-G1-PPI-$(NH_2)_4$ (for **L1**) or DAB-G2-PPI-$(NH_2)_8$ (for **L2**). A broad singlet at ∼8.3 ppm in the ^{1}H NMR spectra for **L1** and **L2** (Figures S1 and S2), which integrates for four and eight protons respectively, is assigned to the imine proton and affirms formation of the Schiff-base. Additional broad multiplets are observed between 1.4 and 3.7 ppm in the ^{1}H NMR spectra for **L1** and **L2**, assigned to the aliphatic of the core and arms of the dendritic ligands. With the aid of 2D-COSY NMR spectra (Figure S4), the aromatic protons of the bpy moieties and the imine protons are more discernible. Furthermore, formation of the imine is confirmed by the diagnostic CH═N absorption band at 1648 cm^{-1} in the IR spectrum for both **L1** and **L2**. Elemental analysis and ESI-mass spectrometry additionally confirmed the integrity of the new ligands.

The peripheral decorated, $Mn(CO)_3$-functionalized tetranuclear (**1**) and octanuclear (**2**) metallodendrimers were synthesized *via* reaction of the ligands **L1** and **L2** with manganese pentacarbonyl bromide (Scheme 1) in dichloromethane at room temperature in the dark. The metallodendrimers **1** and **2** were obtained as yellow-orange solids in moderate yield and purified by preparative RP-HPLC using a gradient of 5−90% CH_3CN/H_2O with 0.1% TFA. The reaction and workup were performed with minimal exposure to light. In the IR spectra of **1** and **2**, three strong peaks appear at about 2020, 1920, and 1900 cm^{-1} as shown in Figure 1 for **1**. With the aid of DFT calculations (*vide infra*), the one at higher wavenumbers is assigned to the symmetrical and the other two to the asymmetrical C≡O-stretching vibrations of the metal-tricarbonyl moiety (see also Table 3). Furthermore, three singlets observed in the $^{13}C\{^1H\}$-NMR spectrum (Figures S8 and S9) at about 220, 221, and 223 ppm also confirm the

Scheme 1. Synthesis of Tetra- and Octanuclear CORM-Dendrimer Conjugates 1 and 2

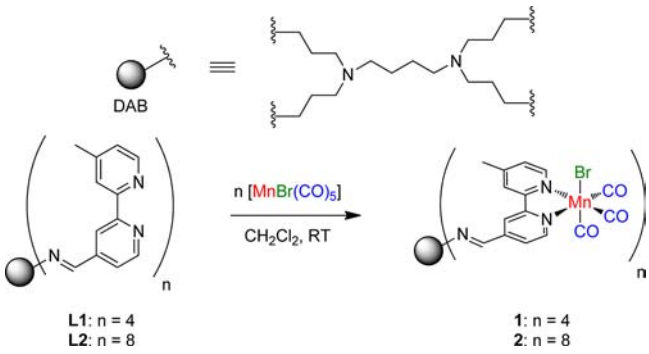

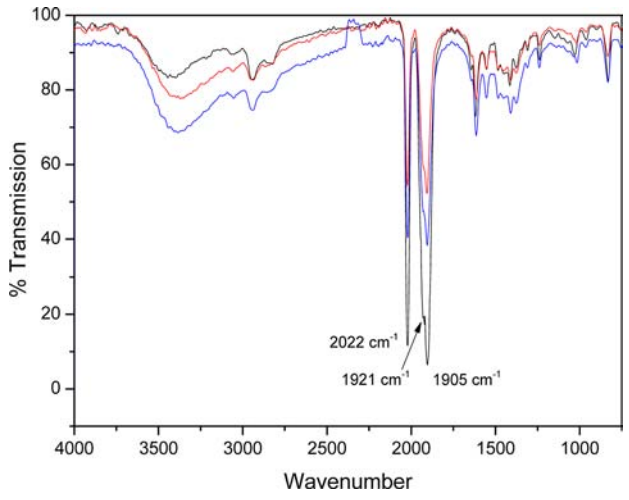

Figure 1. IR (ATR) spectra of dendrimer **1** for a freshly prepared sample (black) and after exposure to daylight for 1.5 h (blue) and 24 h (red).

dx.doi.org/10.1021/ic400377k | Inorg. Chem. 2013, 52, 5470−5478

presence and integrity of the $Mn(CO)_3$ group. The shift to higher wavenumbers of the stretching vibration assigned to the C═N group of the bpy moiety, from 1596 cm^{-1} (ligand) to about 1620 cm^{-1} (complex), indicates that complexation occurred *via* the two pyridyl nitrogen atoms and not *via* the imine nitrogen atom, as there is no shift in the stretching vibration of the imine bond. Broad overlapping signals are observed in the ^1H NMR spectra of **1** and **2** (Figures S5 and S6) and are assigned to the aliphatic protons of the dendritic core and arms, characteristically seen with other similar metallodendrimers.[42−45] HR-ESI-TOF mass spectrometric data further confirmed the structural integrity of metallodendrimers **1** and **2** (Figures S11 and S12).

In addition, mononuclear complex **3** (Scheme 2) was synthesized as a model of the larger metallodendrimers in order to study potential size-dependent scaling effects on the photoactivated CO release. Monomeric ligand **L3** was prepared in a procedure similar to the dendritic ligands (**L1**, **L2**), by reacting 4′-methyl-2,2′-bipyridine-4-carboxaldehyde with *n*-propylamine *via* a Schiff-base condensation reaction. **L3** was further reacted with manganese pentacarbonyl bromide in dichloromethane at room temperature in the absence of light to obtain complex **3** as an orange solid. Complex **3** was purified by preparative HPLC under conditions similar to metallodendrimers **1** and **2**.

Scheme 2. Synthesis of Mononuclear Model Complex 3

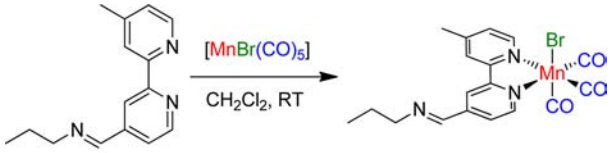

L3 3

For complex **3**, infrared spectral analysis revealed three absorption bands at 2021, 1928, and 1899 cm^{-1}, corresponding to the terminal CO ligands of the $Mn(CO)_3$ fragment. An absorption band observed at 1644 cm^{-1} is assigned the imine bond. HR-ESI-TOF mass spectrometric data confirmed the structural integrity of complex **3**.

Long-Term Stability of Compounds 1−3. When compounds **1**−**3** are exposed to natural daylight for an extended period of time, a pronounced decrease in the intensity of the signals of the $Mn(CO)_3$ moiety between 2025 and 1900 cm^{-1} can be observed (Figures 1 and S13 and S14) in the infrared spectra. This is indicative of significant structural changes in the metal−carbonyl group and a first indicator of the CO release from these compounds.

Electronic Absorption Spectra and CO-Release Properties. The absorbance maxima and molar extinction coefficients of complexes **1**−**3** were determined in a mixture of dimethylsulfoxide and water (10:90% v/v). Two broad bands are observed for all compounds at around 300 nm and, at somewhat lower intensity, in the range of 350−450 nm (Figure 2). With the aid of TDDFT calculations (*vide infra*), these are attributed to interligand charge transfer (ILCT) and metal-to-ligand charge transfer (MLCT), respectively (see also Table 4).

The absorption maxima and the molar extinction coefficients are listed in Table 1. The position of the low-energy MLCT transition at λ_2 increases slightly upon moving from **1** to **2**, by about 10 nm, while the higher energy ILCT band at λ_1 remains unchanged. The increase in molar extinction coefficients for both bands is more pronounced, on moving from the mononuclear model compound **3** to the metallodendrimers **1** and **2**. There is an increase in the molar extinction coefficient by a factor of ∼3.3, on moving from complex **3** to complex **1**. It further doubles on moving from **1** to **2**, which is expected when comparing the increase in the number of $[MnBr(bpy^{CH3,CH=N})(CO)_3]$ groups per compound. This confirms the linear scaling of the optical properties with increasing dendrimer generation.

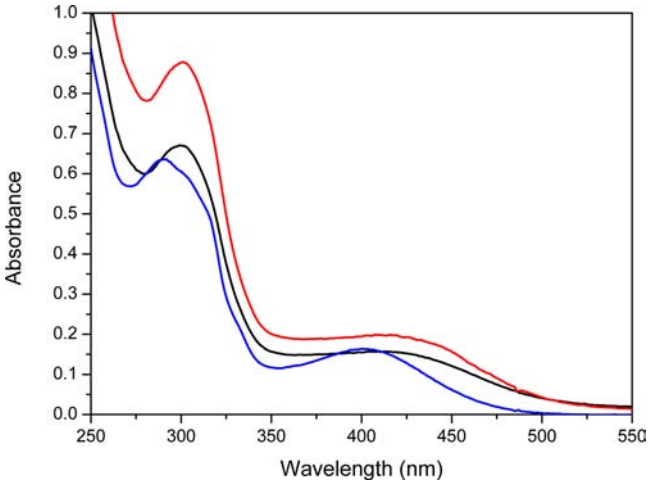

Figure 2. Overlay of the electronic absorption spectra of complexes **1** (black), **2** (red), and **3** (blue) in dimethylsulfoxide/water (10:90% v/v).

Table 1. Absorption Maxima and Molar Extinction Coefficient of Complexes 1−3

compound	absorption maxima λ_1 [nm]	ε_1 [M^{-1} cm^{-1}]	absorption maxima λ_2 [nm]	ε_2 [M^{-1} cm^{-1}]
1	300	47 717 ± 1413	410	10 371 ± 550
2	300	91 606 ± 657	420	18 799 ± 818
3	290	13 278 ± 370	400	3527 ± 194

To obtain insight into the dark stability and photoinduced CO-release from compounds **1**−**3**, these complexes were first incubated in dimethylsulfoxide/water (10:90% v/v) solution in the absence of light for an extended period of time and then irradiated with a custom-made LED cluster at 410 nm, coincident with the MLCT absorption maximum. Irradiations were interrupted in 1 min intervals to measure UV/vis spectra. All three compounds showed good dark stability in aqueous solution for up to 15 h with only negligible spectral fluctuations observed at around 300 and 410 nm (Figures S15−S20). In stark contrast, irradiation at 410 nm resulted in a pronounced decrease of the broad band centered at around 400 nm to almost zero toward the end of the experiment and a blue-shift of the peak at around 300 nm. Plateau values were reached after about 10−15 min with no further spectral changes upon extended irradiation.

CO-Release Experiments with the Myoglobin Assay. The CO release from compounds **1**−**3** was then studied using the standard myoglobin assay, which is based on the UV/vis spectroscopic detection of the conversion of deoxyMb to MbCO (Mb = myoglobin).[46,47] However, prior to the irradiation experiments, the stability of **1**−**3** in 0.1 M phosphate buffer (PBS, pH 7.4) under the reducing conditions of the myoglobin assay was monitored using UV/vis spectroscopy.

dx.doi.org/10.1021/ic400377k | Inorg. Chem. 2013, 52, 5470−5478

The two metallodendrimers **1** and **2** showed negligible spectral changes over 12−16 h when monitored at four different wavelengths in the Q-band region of myoglobin, between 500 and 600 nm (Figures 3 and S21). This indicates that no CO release to myoglobin occurs in the dark during this time and is a good indicator of the suitability of these compounds as photoactivatable CO-prodrugs. For model compound **3**, some minor fluctuations were observed in the same spectral region (Figure S22), in particular during the first few hours of incubation, but since these affected all wavelengths monitored to the same degree, they are probably rather indicative of some precipitation due to poor solubility than a general instability of the compound.

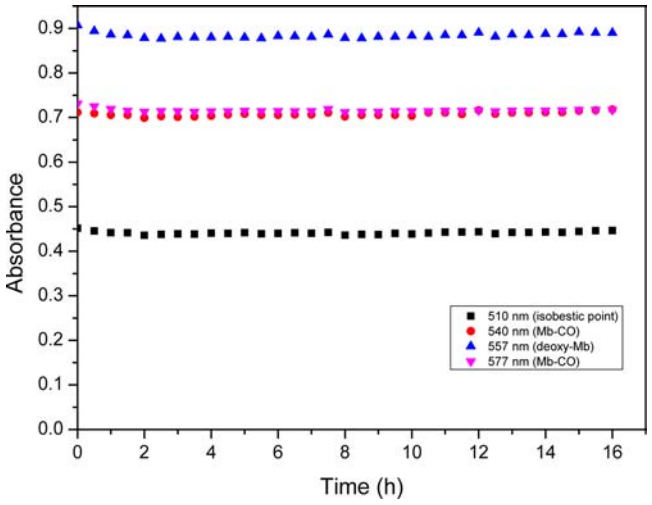

Figure 3. Change of absorption at selected wavelengths with increasing incubation time in the dark (0 to 16 h) for a solution of dendrimer **1** (4 μM) in 0.1 M PBS at pH 7.4 in the presence of myoglobin (60 μM) and sodium dithionite (10 mM) under a dinitrogen atmosphere as monitored by UV/vis spectroscopy.

For photoactivation studies, a custom-made LED cluster with an emission wavelength of 410 nm, matching the MLCT band, was used. The violet light photoactivation of the present compounds **1**-**3** is quite an attractive feature, since most PhotoCORMs reported to date only show sensitivity to light at shorter wavelengths (315−365 nm).[31,34,48−50] For deep tissue penetration, an excitation wavelength of larger than 600−700 nm would be ideal, which would also minimize potential photodamage to healthy cells.[51] By suitable modification of the substituents in the 4-position of the bipyridine ligand, it is anticipated that the excitation wavelength can be further shifted toward the red. The photoexcitation at 410 nm leads to pronounced changes in the Q-band region of the Mb absorption. The band at 557 nm slowly decreases in intensity while two new bands at 540 and 577 nm slowly increases in intensity, which is characteristic for the conversion of deoxyMb to MbCO (Figures 4 and S23 and S24).

The concentration of MbCO in solution was determined from the absorption data by application of the Beer−Lambert law using a molar extinction coefficient for MbCO of $\lambda_{540\ nm}$ = 15.4 $(mM)^{-1}$ L^{-1}.[52] Since the concentration of deoxyMb has to be fixed to keep the absorption in the Q-band region <1, an excess of deoxyMb over the total amount of potentially labile CO in **1**−**3** was always maintained. When 4 μM of **1** was added to 60 μM of deoxy-Mb, the CO-release profile of complex **1** upon photoactivation (Figure 5) indicates that approximately eight CO ligands are released per molecule of **1** (Table 2), with a $t_{1/2}$ of 14.5 min. Second-generation metallodendrimer **2** (2 μM) released a significantly higher number of CO ligands, about 15 equivalents (Figure S25), but only shows a marginally increased half-life of 16.8 min. For the mononuclear model complex **3** (10 μM), about two CO ligands per molecule were released upon exhaustive photoactivation (Figure S26, Table 2), with a significantly shortened $t_{1/2}$ of 7.4 min. The $t_{1/2}$ in this study is defined as the time taken for compounds **1**−**3** to release 50% of the total CO ligands present per molecule. While the absolute number of CO ligands liberated from the molecules increases from about 1.5 to 15.2 when comparing **1**−**3**, interestingly, the proportional amount of CO released vs the remaining bound CO stays remarkably constant, with an average value of ~65% for the two metallodendrimers (**1**, **2**)

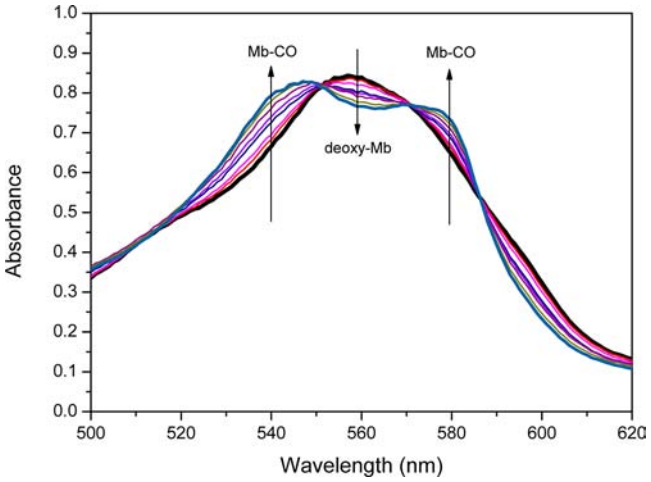

Figure 4. Change of absorption in the Q-band region of myoglobin with increasing irradiation time at 410 nm for a solution of dendrimer (4 μM) in 0.1 M PBS pH 7.4 in the presence of myoglobin (60 μM) and sodium dithionite (10 mM) under a dinitrogen atmosphere as monitored by UV/vis spectroscopy.

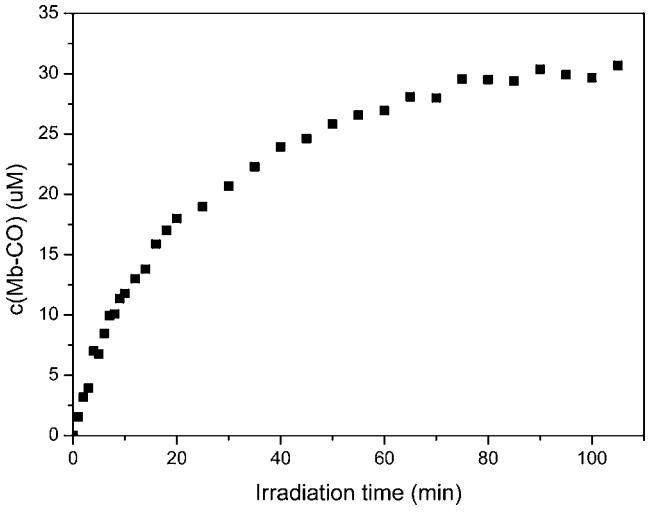

Figure 5. Amount of MbCO in μM formed with increasing irradiation time at 410 nm for a solution of compound **1** (4 μM) in 0.1 M PBS at pH 7.4 in the presence of myoglobin (60 μM) and sodium dithionite (10 mM) under a dinitrogen atmosphere as determined from UV/vis spectroscopy.

dx.doi.org/10.1021/ic400377k | Inorg. Chem. 2013, 52, 5470−5478

Table 2. CO-Release and Kinetic Data for Complexes 1−3

complex	conc. of MbCO [μM]	half-life, $t_{1/2}$ [min][a]	rate constant, k_{CO} [s^{-1}][b]	equiv. of CO released[c]	percentage CO released [%][c]	quantum yield, Φ_{410}[d]
1	30.24 ± 0.08	14.54 ± 0.25	0.000795	7.56 ± 0.02	63.0	(2.66 ± 0.16) × 10^{-3}
2	30.47 ± 0.31	16.84 ± 0.56	0.000686	15.24 ± 0.15	63.5	(2.71 ± 0.49) × 10^{-3}
3	20.29 ± 3.03	7.41 ± 0.24	0.001558	1.51 ± 0.07	50.5	(3.15 ± 0.27) × 10^{-3}

[a]Determined under the conditions of the myoglobin assay. [b]Determined from UV/vis spectral studies in DMSO/water solution. [c]Per molecule. [d]Calculated using a photon flux of the LED array determined as (9.9 ± 0.4) × 10^{-9} Einstein·s^{-1}

and ∼51% for the mononuclear complex **3**. Thus, under the conditions of the myoglobin assay, a maximum of two out of the three CO ligands per metal carbonyl moiety are photolabile. Furthermore, these data indicate that the CO release from the different $Mn(CO)_3$ groups in the dendrimers does not seem to be a cooperative process due to the linear scaling.

Kinetics and Quantum Yield Measurements. The rate of CO release from compounds **1**−**3** was determined in dimethylsulfoxide/water (10:90% v/v) by recording changes in the electronic absorption spectrum of each compound at selected wavelengths (**1** at 410 nm, **2** at 420 nm, and **3** at 400 nm) during irradiation with a LED array at 410 nm for predefined time intervals. It follows a pseudo first-order behavior and is listed in Table 2. All three compounds show CO-release rates (k_{CO}) comparable to $[Mn(tpm)(CO)_3]^+$,[32] one of the first PhotoCORMs reported, and relatively faster rates than other manganese-functionalized CORMs reported so far.[49,53,54] Also, in comparison to other metal carbonyl complexes such as the iron compound $[Fe(CO)(N4Py)](ClO_4)_2$, CO-release rates are comparable.[55]

The apparent quantum yield of CO release under the conditions of the myoglobin assay was determined by ferrioxalate actinometry.[56,57] While the values of Φ are essentially identical for the two dendrimer conjugates **1** and **2** at about 2.7 × 10^{-3}, again indicating that scaling effects do not play any role in these systems, for the model compound **3**, a slightly larger value of 3.2 × 10^{-3} was determined. These values are much lower than reported for other metal carbonyl complexes by 1 to 2 orders of magnitude.[24,49,58] However, one has to take into account that our experiments were not carried out in pure solvent, but rather under the conditions of the myoglobin assay, using an excitation wavelength of 410 nm, in a spectral region where substantial absorption of the heme protein leads to considerable inner filter effects.

DFT and TDDFT Calculations. In order to obtain a degree of insight into the electronic structure of the metal complex unit and the optical transitions involved in the CO-release process, DFT and TDDFT calculations were carried out on the full molecular unit of **3** without any simplification using the ORCA program package with the RI-BP86 (geometry optimization and calculation of vibrational frequencies) or RIJCOSX-B3LYP functionals (TDDFT) and a TZVP basis set on all atoms in both cases, taking into account the solvent (water) with the COSMO model. In addition to the structure of **3** as shown in Scheme 2 with the bromide ligand perpendicular to the plane of the bipyridine and the three carbonyl ligands in a facial arrangement (**3-A**, here termed as the "axial" isomer), also the two meridional isomers with the Br group in plane with the bpy ligand ("equatorial"), either *trans* to the imine (**3-B**) or *trans* to the methyl group (**3-C**), were optimized and characterized as minima due to the absence of imaginary modes in the calculated vibrational spectra. However, not unexpectedly, the two *mer*-isomers were higher in energy compared to the axial one (**3-A**) by 103 and 107 kJ mol^{-1} for **3-B** and **3-C**, respectively, and thus not further considered (Figure S27). The calculated bond distances and angles of $[MnBr(bpy^{R,R'})(CO)_3]$ (**3**) showed good accordance with the values of the reported X-ray structures of closely related complexes $[MnX(bpy)(CO)_3]$ with X = Cl and I (Table S1).[59,60] As also observed for other RI-BP86 studies on metal carbonyl complexes, the calculated Mn−N/C/X bond distances were too short compared to the X-ray data by about 0.10 Å (or 5.6%) while the C≡O bond distances were too long by about 0.04 Å (3.3%) and the average deviation in the bond angles of an order of 0.1° (or 1.3%). However, with an average difference of 2.6% over all parameters evaluated, the DFT reproduction of structural data has to be considered as excellent.

The calculated vibrational frequencies showed no imaginary modes but significantly deviated from the experimental values and thus were multiplied with a scaling factor of 1.021.[61−63] They are collected in Table 3 for all three isomers **3-A/B/C** calculated and compared to the experimental ones.

Table 3. Comparison of Major Experimental and Scaled Calculated Vibrational Frequencies for 3-A/B/C, Absolute Values, and Deviation from Experimental Ones in Parentheses (all in cm^{-1})

mode	**3** exptl.	**3-A** calcd.	**3-B** calcd.	**3-C** calcd.
ν(CH═N)	1644	1674 (+30)	1671 (+27)	1675 (+31)
ν_{asym1}(C≡O)	1899	1878 (−21)	1882 (−17)	1880 (−19)
ν_{asym2}(C≡O)	1928	1882 (−46)	1907 (−21)	1903 (−25)
ν_{sym}(C≡O)	2021	2007 (−14)	2025 (+4)	2022 (+1)

The mode at highest wavenumbers, slightly above 2000 cm^{-1}, is assigned to the symmetrical C≡O stretching vibration of the *fac*-$Mn(CO)_3$, moiety while in the 1880−1930 cm^{-1} range, there are two asymmetrical C≡O stretches due to the low symmetry of the compound. The C═N stretch of the imine is found lowest, at around 1660 cm^{-1}. While the latter is overestimated in the model chemistry used by about 30 cm^{-1}, the metal−carbonyl C≡O stretches are mostly underestimated by around 10 to 50 cm^{-1}, with a somewhat smaller deviation on the symmetrical compared to the asymmetrical stretch. However, the calculated values of the vibrations of the three isomers **3A**, **3B**, and **3C** are all very similar among themselves and also to the experimental data that one cannot rely on this type of DFT calculations to assign the kind of isomer present. The first 45 singlet excited states were then calculated with TDDFT for the facial isomer **3-A**, and the most prominent states are listed in Table 4.

In line with the presence of a low-spin $3d^6$ metal center, the HOMO to HOMO−2 orbitals are mostly of Mn d character, but with significant admixture from CO π and Br p orbitals. The HOMO−3 is a bpy-centered π orbital and the HOMO−4/−5 a mix of bromide p and imine N lone-pair character, followed by more orbitals of mixed Br/bpy contributions. The

dx.doi.org/10.1021/ic400377k | Inorg. Chem. 2013, 52, 5470−5478

Table 4. Energies (in nm), Oscillator Strength (f_{osc}), Main Orbital Contributions, and Type of Transition Involved in the Most Important Singlet Excitations for 3-A Calculated with TDDFT

state[a]	λ nm	f_{osc}	main transitions[b]	type of transition
2	506.2	0.1190	113→115 (79%)	MLCT Mn→bpy
4	441.4	0.0535	113→116 (29%)	MLCT Mn→bpy
			114→116 (62%)	
5	431.2	0.0829	113→116 (65%)	MLCT Mn→bpy
			114→116 (23%)	
7	372.5	0.0182	114→117 (77%)	MLCT Mn→bpy (py^{CH3} part)
9	351.2	0.0178	113→117 (75%)	MLCT Mn→bpy (py^{CH3} part)
10	343.0	0.0297	108→115 (67%)	LLCT Br→bpy (py^{imine} part)
			111→115 (27%)	
11	328.7	0.1895	109→115 (23%)	LLCT Br→bpy
			110→115 (53%)	
12[c]	305.6	0.2189	111→115 (38%)	MLCT Mn→bpy
13[c]	320.9	0.0385	112→117 (84%)	MLCT Mn→bpy (py^{CH3} part)

[a]Only strong transitions with an oscillator strength >0.01 in the 300–600 nm range are reported. [b]Only contributions >20% are listed. [c]The reversed order is due to state 13 experiencing a much smaller solvent shift than the others.

LUMO to LUMO+2 are bpy π^* orbitals, and at even higher energies, orbitals have a mixed Mn/Br/CO/bpy contribution.

Inspection of the difference densities of states calculated to be closest to the excitation wavelength of 410 nm (in particular states 4 and 5) shows that these are mostly of Mn-to-bpy MLCT character (Figure 6). This should lead to a decrease of electron density on the metal center in the excited state, with a subsequent decrease in backdonation to the CO π^* orbitals and thus a weakening of the M–CO bond, facilitating CO release from the metal coordination sphere, as already demonstrated for other manganese-based PhotoCORMs.[64]

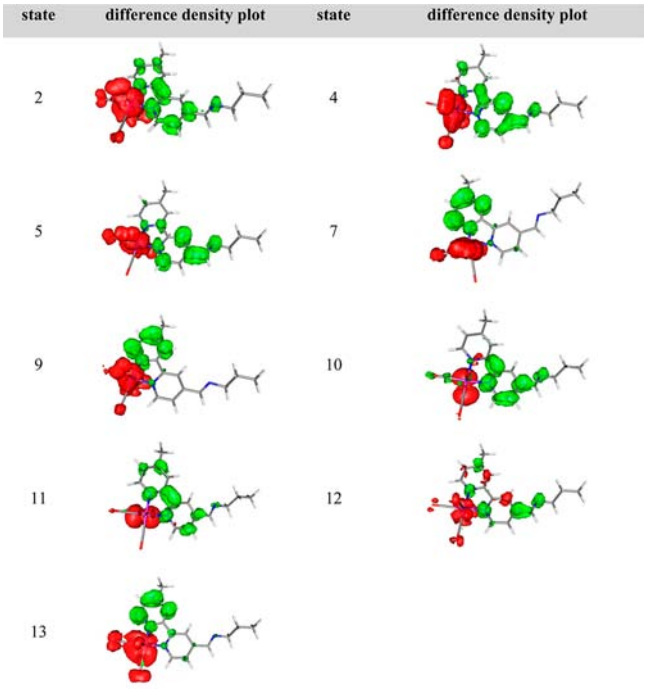

Figure 6. TDDFT difference densities for the most important singlet excitations for **3-A** in the 300 to 600 nm range. Isosurface values are plotted at ±0.002, with positive values shown in green and negative ones in red.

EXPERIMENTAL SECTION

General Procedures. All organic reactants were purchased either from Sigma-Aldrich or from Fluka and were used as received unless otherwise stated. Manganese pentacarbonyl bromide [$MnBr(CO)_5$] was obtained from Strem Chemicals. 4′-Methyl-2,2′-bipyridine-4-carboxaldehyde was prepared according to literature methods.[65,66] Infrared spectra were recorded either using a Perkin-Elmer Spectrum 100 FT-IR spectrometer using NaCl solution cells in dichloromethane (**L1**–**L3**) or as pure solid samples using a Nicolet 380 FT-IR-Spectrometer equipped with a SMART iTR ATR unit (**1**–**3**). Intensities of stretching vibrations are marked as strong (s), medium (m), or weak (w). Elemental analysis (C, H, N) was carried out using a Thermo Flash 1112 Series CHNS-O Analyzer. HPLC analysis was done on a Dionex Ultimate 3000 instrument equipped with a ReproSil 100 column (C_{18}, 5 μm, 4.6 mm or 10 mm diameter, 250 mm length) using a linear gradient of 5–90% acetonitrile/water containing 0.1% TFA as the eluent over 40 min at a flow rate of 0.6 mL/min for analytical and 3.0 mL/min for preparative chromatography, respectively. Nuclear magnetic resonance (NMR) spectra were recorded on a Varian Unity XR400 spectrometer (^{1}H, 399.95 MHz; $^{13}C\{^1H\}$, 100.58 MHz) or a Bruker Avance 500 spectrometer (^{1}H, 500.13 MHz, $^{13}C\{^1H\}$, 125.77 MHz) at ambient temperature. Chemical shifts δ in parts per million indicate a downfield shift relative to tetramethylsilane (TMS) and were referenced relative to the signal of the solvent.[67] Coupling constants J are given in hertz. Individual peaks are marked as singlet (s), doublet (d), doublet-of-doublet (dd), triplet (t), or multiplet (m). Absorption spectra were measured using an Agilent 8453 UV/vis diode array spectrophotometer in quartz cuvettes (d = 1 cm). Electrospray ionization-mass spectrometry (ESI-MS) was carried out on a Waters Synapt mass spectrometer. Data were recorded in positive ion mode. Electron impact mass spectrometry (EI-MS) was carried out on a JEOL GCmateII mass spectrometer.

Synthesis of Bipyridyl Ligands (L1–L3). A solution of DAB-G1-PPI-$(NH_2)_4$ (0.481 g, 1.51 mmol for **L1**), DAB-G2-PPI-$(NH_2)_8$ (0.822 g, 1.06 mmol for **L2**), or *n*-propylamine (0.360 g, 6.08 mmol for **L3**) in dichloromethane (10 mL) was added dropwise to a stirred solution of 4′-methyl-2,2′-bipyridine-4-carboxaldehyde (1.22 g, 6.15 mmol for **L1**; 1.70 g, 8.56 mmol for **L2**; 1.21 g, 6.39 mmol for **L3**) in dichloromethane (25 mL) and stirred for 48 h (for **1** and **2**) or overnight (for **3**) at room temperature (with DAB = 1,4-diaminobutane, PPI = poly(propyleneimine)). The solvent was then removed under vacuum conditions to afford a dark yellow oil. This was dissolved in dichloromethane (30 mL) and washed with copious amounts of ultrapure water (15 × 30 mL). The organic layer was separated, dried over sodium sulfate (~10 g), and filtered. The solvent was then removed under reduced pressure and the resulting oil dried *in vacuo*.

[DAB-G1-PPI-$(bpy^{CH3,CH=N})_4$] ***L1***. Red-brown oil, yield: 1.41 g, 89.5%. IR, NaCl cell, CH_2Cl_2, ν/cm^{-1}: 1648 (s, imine, C=N), 1596 (s, pyridyl, C=N). ^{1}H NMR ($CDCl_3$): δ (ppm) 1.45 (br m, 4H, NCH_2CH_2 core), 1.84 (br m, 8H, $NCH_2CH_2CH_2N_{branch}$), 2.42 (s, 16H, NCH_2CH_2core, CH_3), 2.52 (br m, 8H, $NCH_2CH_2CH_2N_{branch}$), 3.68 (br m, 8H, $NCH_2CH_2CH_2N_{branch}$), 7.11 (br d, ^3J = 4.8 Hz, 4H, CH_{bpy}), 7.64 (br d, ^3J = 5.0 Hz, 4H, CH_{bpy}), 8.21 (br s, 4H, CH_{bpy}), 8.33 (br s, 4H, CH_{imine}), 8.51 (br d, ^3J = 4.9 Hz, 4H, CH_{bpy}), 8.56 (br s, 4H, CH_{bpy}), 8.67 (br d, ^3J = 5.0 Hz, 4H, CH_{bpy}). $^{13}C\{^1H\}$ NMR ($CDCl_3$): δ (ppm) 21.2 (CH_3); 25.3, 28.4, 51.7, 54.1, 59.9 (CH_2); 120.5, 120.9, 122.0, 124.9, 149.1, 149.6 (CH_{pyr}); 144.2, 148.1, 155.6, 157.2 (C_{pyr}); 159.3 (CH_{imine}). Elemental analysis for $C_{64}H_{72}N_{14}$ (1037.37), found: C, 73.92; H, 7.11; N, 18.97%. Calcd.: C, 74.10; H, 7.00; N, 18.90%. MS (HR-ESI-TOF, m/z): 1038.79 $[M + H]^+$.

[DAB-G2-PPI-$(bpy^{CH3,CH=N})_8$] ***L2***. Red-brown oil, yield: 2.09 g, 88.7%. IR, NaCl cells, CH_2Cl_2, ν/cm^{-1}: 1648 (s, imine, C=N), 1596

dx.doi.org/10.1021/ic400377k | Inorg. Chem. 2013, 52, 5470–5478

(s, pyridyl, C═N). ^{1}H NMR ($CDCl_3$): δ (ppm) 1.39 (br m, 4H, NCH_2CH_{2core}), 1.57 (br m, 8H, $NCH_2CH_2CH_2N_{firstbranch}$), 1.83 (br m, 16H, $NCH_2CH_2CH_2N_{secondbranch}$), 2.31 - 2.59 (overlapping m, 60H, NCH_2CH_{2core}, $NCH_2CH_2CH_2N_{firstbranch}$, $NCH_2CH_2CH_2N_{firstbranch}$, $NCH_2CH_2CH_2N_{secondbranch}$, CH_3), 3.65 (br m, 16H, $NCH_2CH_2CH_2N_{secondbranch}$), 7.09 (br m, 8H, CH_{bpy}), 7.62 (br d, 8H, ^3J = 5.0 Hz, CH_{bpy}), 8.19 (br s, 8H, CH_{bpy}), 8.30 (br s, 8H, CH_{imine}), 8.49 (br d, ^3J = 4.9 Hz 8H, CH_{bpy}), 8.56 (br s, 8H, CH_{bpy}), 8.64 (br d, ^3J = 5.0 Hz, 8H, CH_{bpy}). $^{13}C\{^1H\}$ NMR ($CDCl_3$): δ (ppm) = 21.1 (CH_3); 24.7, 25.2, 28.3, 51.7, 52.3, 53.4, 54.2, 59.9 (CH_2); 120.4, 120.9, 121.9, 124.8, 149.0, 149.5 (CH_{pyr}); 144.2, 148.1, 155.6, 157.2 (C_{pyr}); 159.2 (CH_{imine}). Elemental analysis for $C_{136}H_{160}N_{30}$ (2214.96), found: C, 73.74; H, 7.58; N, 18.68%. Calcd.: C, 73.75; H, 7.28; N, 18.97%. MS (HR-ESI-TOF, m/z): 560.25 $[M + 4H]^{4+}$

*[bpy$^{CH3,CH=NCH2CH2CH3}$] **L3***. Dark yellow oil, yield: 0.920 g, 63.2%. IR, NaCl cells, CH_2Cl_2, ν/cm^{-1}: 1649 (s, imine, C═N), 1596 (s, pyridyl, C═N). ^{1}H NMR ($CDCl_3$): δ (ppm) 0.94 (t, ^3J = 7.4 Hz, 3H, $NCH_2CH_2CH_3$), 1.73 (m, 2H, $NCH_2CH_2CH_3$), 2.41 (s, 3H,CH_{3bpy}), 4.20 (td, ^3J = 6.9 Hz, ^4J = 1.4 Hz, 2H, $NCH_2CH_2CH_3$), 7.11 (d, ^3J = 2.4 Hz, 1H, CH_{bpy}), 7.67 (dd, ^3J = 5.0 Hz, ^4J = 1.6 Hz, 1H, CH_{bpy}), 8.22 (s, 1H, CH_{bpy}), 8.32 (s, 1H, CH_{imine}), 8.52 (d, ^3J = 5.4 Hz, 1H, CH_{bpy}), 8.58 (s, 1H, CH_{bpy}), 8.69 (d, ^3J = 5.26 Hz, 1H, CH_{bpy}). $^{13}C\{^1H\}$ NMR ($CDCl_3$): δ (ppm) 11.8, 21.1 (CH_3); 23.8, 63.6 (CH_2); 120.5, 120.9, 122.0, 124.9, 149.0, 149.5 (CH_{pyr}); 144.3, 148.1, 155.6, 157.2 (C_{pyr}); 159.1 (CH_{imine}). Elemental analysis for $C_{15}H_{17}N_3$ (239.32), found: C, 75.26; H, 7.19; N, 17.55%. Calcd.: C, 75.28; H, 7.16; N, 17.56%. MS (EI, m/z): 239.28 $[M]^+$.

Synthesis of Mn(CO)$_3$-Functionalized Metallodendrimers (1−3). A solution of ligand **L1** (0.112 g, 0.108 mmol for **1**), **L2** (0.116 g, 0.053 mmol for **2**), or **L3** (0.103 g, 0.429 mmol for **3**) in dichloromethane (5 mL) was added dropwise to a stirred suspension of $[MnBr(CO)_5]$ (0.120 g, 0.439 mmol for **1**, 0.116 g, 0.423 mmol for **2**, and 0.112 g, 0.408 mmol for **3**) in dichloromethane (30 mL). The reaction mixture was stirred overnight at room temperature while protected from light by wrapping it in aluminum foil, then filtered by gravity, and the filtrate was reduced to ∼5 mL. The addition of diethyl ether (for **1** and **2**) or *n*-pentane (for **3**) led to precipitation of the desired product. The solids were filtered, washed with copious amounts of diethyl ether or *n*-pentane, and dried under vacuum conditions. Single crystals of complex **3** were obtained by slow diffusion of *n*-pentane into a concentrated dichloromethane solution of the compound but did not diffract well enough for a good structure solution due to disorder.

*[DAB-G1-PPI-{MnBr(bpy$^{CH3,CH=N}$)(CO)$_3$}$_4$] **1***. Yellow-orange solid, yield: 0.165 g, 79.1%. IR, ATR, ν/cm^{-1}: 2022 (s, carbonyl, C≡O), 1921 (s, carbonyl, C≡O), 1905 (s, carbonyl, C≡O), 1644 (m, imine, C═N), 1618 (m, bpy, C═N). ^{1}H NMR ($(CD_3)_2SO$): δ (ppm) 1.39 (overlapping m, 12H, NCH_2CH_{2core}, $NCH_2CH_2CH_2N_{branch}$), 1.77 (overlapping m, 12H, NCH_2CH_{2core}, $NCH_2CH_2CH_2N_{branch}$), 2.36 (br m, 12H, CH_3), 3.69 (br m, 8H, $NCH_2CH_2CH_2N_{branch}$), 7.52 (br m, 4H, CH_{bpy}), 7.89 (br m, 4H, CH_{bpy}), 8.46 (br s, 4H, CH_{imine}), 8.51 (br s, 4H, CH_{bpy}), 8.76 (br s, 4H, CH_{bpy}), 8.98 (br m, 4H, CH_{bpy}), 9.19 (br m, 4H, CH_{bpy}). $^{13}C\{^1H\}$ NMR ($(CD_3)_2SO$): δ (ppm) 20.6 (CH_3); 24.7, 27.8, 50.9, 53.4, 58.9 (CH_2); 121.0, 123.5, 124.2, 127.8, 153.9, 154.3 (CH_{Ar}); 145.2, 151.2, 152.8, 156.0 (C_{Ar}); 158.0 (CH_{imine}); 221.0, 221.7, 222.0 (CO). HPLC (CH_3CN/H_2O (gradient, 5−90%, flow rate, 0.6 mL/min): t_R = 23.1 min. MS (HR-ESI-TOF, m/z): 961.57 $[M + 2H]^{2+}$.

*[DAB-G2-PPI-{MnBr(bpy$^{CH3,CH=N}$)(CO)$_3$}$_8$] **2***. Yellow-orange solid, yield: 0.139 g, 65.4%. IR, ATR, ν/cm^{-1}: 2022 (s, carbonyl, C≡O), 1920 (s, carbonyl, C≡O), 1904 (s, carbonyl, C≡O), 1644 (m, imine, C═N), 1619 (m, bpy, C═N). ^{1}H NMR ($(CD_3)_2SO$): δ (ppm) 1.23 (overlapping m, 28H, NCH_2CH_{2core}, $NCH_2CH_2CH_2N_{firstbranch}$, $NCH_2CH_2CH_2N_{secondbranch}$), 1.38 (overlapping m, 20H, NCH_2CH_{2core}, $NCH_2CH_2CH_2N_{firstbranch}$, $NCH_2CH_2CH_2N_{firstbranch}$), 1.71 (br m, 16H, $NCH_2CH_2CH_2N_{secondbranch}$), 2.42 (br m, 24H, CH_3), 3.63 (br m, 16H, $NCH_2CH_2CH_2N_{secondbranch}$), 7.48 (br m, 8H, CH_{bpy}), 7.84 (br m, 8H, CH_{bpy}), 8.43 (br m, 16H, CH_{imine}, CH_{bpy}), 8.69 (br s, 8H, CH_{bpy}), 8.95 (br m, 8H, CH_{bpy}), 9.14 (br m, 8H, CH_{bpy}). $^{13}C\{^1H\}$ NMR ($(CD_3)_2SO$): δ (ppm) 20.6 (CH_3); 24.2, 24.9, 27.8, 51.0, 51.5, 53.8, 54.7, 58.9 (CH_2); 121.0, 123.4, 124.1, 127.8, 153.8, 154.3 (CH_{Ar}); 145.2, 151.1, 152.8, 156.0 (C_{Ar}); 157.8 (CH_{imine}); 220.9, 221.6, 222.9 (CO). HPLC (CH_3CN/H_2O (gradient, 5−90%, flow rate, 0.6 mL/min): t_R = 23.1 min. MS (HR-ESI-TOF, m/z): 1344.59 $[M + 3H]^{3+}$.

*[MnBr(bpy$^{CH3,CH=NCH2CH2CH3}$)(CO)$_3$] **3***. Orange solid, yield: 0.0731 g, 39.1%. IR, ATR, ν/cm^{-1}: 2021 (s, carbonyl, C≡O), 1928 (s, carbonyl, C≡O), 1899 (s, carbonyl, C≡O), 1644 (m, imine, C═N), 1616 (m, bpy, C═N). ^{1}H NMR ($(CD_3)_2SO$): δ (ppm) 0.93 (br t, ^3J = 6.85 Hz, 3H, $NCH_2CH_2CH_3$), 1.72 (br m, 2H, $NCH_2CH_2CH_3$), 2.55 (br s, 3H, CH_{3bpy}), 3.69 (br t, ^3J = 6.23 Hz, 2H, $NCH_2CH_2CH_3$), 7.58 (br m, 1H, CH_{bpy}), 7.97 (br m, 1H, CH_{bpy}), 8.53 (br s, 1H, CH_{imine}), 8.59 (br s, 1H, CH_{bpy}), 8.82 (br s, 1H, CH_{bpy}), 9.02 (br m, 1H, CH_{bpy}), 9.25 (br m, 1H, CH_{bpy}). $^{13}C\{^1H\}$ NMR ($(CD_3)_2SO$): δ (ppm) 11.7, 20.6 (CH_3); 23.3, 62.5 (CH_2); 120.9, 124.0, 124.3, 127.9, 154.1, 154.4 (CH_{Ar}); 145.4, 151.3, 152.8, 158.1 (C_{Ar}); 158.2 (CH_{imine}); 221.0, 221.7, 222.0 (CO). HPLC (CH_3CN/H_2O (gradient, 5−90%, flow rate, 0.6 mL/min): t_R = 22.9 min. MS (HR-ESI-TOF, m/z): 462.02 $[M+H]^+$.

Myoglobin Assay. A solution of horse skeletal muscle myoglobin in phosphate buffer (PBS, 0.1 M, pH 7.4) was degassed by bubbling with dinitrogen and reduced by the addition of sodium dithionite (100 mM, 100 μL) in PBS buffer (0.1 M, pH 7.4). A concentrated stock solution of metal compounds **1**, **2**, or **3** in dimethylsulfoxide/water (10:90, v/v) was added, followed by PBS to give a total volume of 1000 μL and final concentrations of 60 μM of myoglobin, 10 mM of sodium dithionite and 4 μM of **1**, 2 μM of **2**, or 10 μM of **3**. Solutions were freshly prepared for the dark stability and photoactivation experiments. Irradiations were carried out under dinitrogen with a custom-built LED setup at 410 nm (5 mm round type UV-LEDs, wavelength range 407−412 nm, model YDG-504VC, Kingbright Elec. Co., Taipei, Taiwan, http://www.kingbright.com, part no. 181000−05), positioned perpendicular to the cuvette at a distance of 5 cm. The irradiation was interrupted in 1 min intervals during the initial 10 min, followed by 2 min intervals for the next 10 min, and then 5 min intervals to collect UV/vis spectra on an Agilent 8453 UV/vis diode array spectrophotometer until no more spectral changes were observed in the Q-band region of myoglobin. Dark control spectra were automatically collected for an extended period of time set by the spectrometer software. All irradiation experiments were carried out in triplicate.

Ferrioxalate Actinometry. Ferrioxalate actinometry was used to determine the photon flux of the 410 nm LED array because of its sensitivity, wide spectral range including ultraviolet, and ease of use.[56,57] The entire ferrioxalate actinometry procedure including the preparation of solutions was carried out under dim red light. The moles of ferrous iron formed were determined spectrophotometrically by complexation with 1,10-phenanthroline (phen) to give the colored tris-phenanthroline complex, $[Fe(phen)_3]^{2+}$ with λ_{max} = 510 nm. In a 1 cm quartz cell, 0.006 M (3 mL) of potassium ferrioxalate in 0.05 M sulfuric acid as the chemical actinometer was irradiated with a 410 nm LED array under efficient stirring. A total of 1 ml of this irradiated solution was mixed with 0.1% 1,10-phenanthroline in water and 0.5 mL of sodium acetate buffer in water (1 M, pH 3.5) and further diluted to 10 mL by water. A reference was prepared in the same way except that it was not irradiated. Both solutions were placed in the dark (about an hour) to allow the complexation to complete. The absorbance was then measured at 510 nm (ε = 11.100 M^{-1} cm^{-1}). A_{510} was kept within the range of 0.4−1.0. The photon flux of the 410 nm LED array was then calculated by using $\Phi_{410\ nm}$ = 1.14 following the equation:[68]

$$\varnothing_p = \frac{\Delta A \cdot V_1 \cdot 10^{-3} \cdot V_3}{\varnothing_\lambda \cdot \varepsilon_{510} \cdot V_2 \cdot t}$$

Density Functional Theory Calculations. DFT calculations were carried out on the Linux cluster of the Leibniz-Rechenzentrum (LRZ) in Munich with ORCA version 2.8,[69] using the BP86 functional with the resolution-of-the-identity (RI) approximation, a def2-TZVP/def2-TZVP/J basis set,[70,71] the tightscf and grid4 options, and the COSMO solvation model with water as the solvent for geometry

dx.doi.org/10.1021/ic400377k | Inorg. Chem. 2013, 52, 5470−5478

optimizations and subsequent calculation of vibrational frequencies to characterize the structures obtained as minima by inspection for the absence of imaginary modes. The TDDFT calculations employed the B3LYP functional with the same basis set and settings as above using the RIJCOSX keyword. The first 45 singlet excited states were calculated (nroots 45).

CONCLUSION

In the present paper, first- and second-generation polypyridyl dendritic ligands were synthesized and fully characterized. Subsequent complexation of the 2,2′-bipyridine dendritic ligands to manganese pentacarbonyl bromide gave metallodendrimers with four and eight $[MnBr(bpy^{CH3,CH=N})(CO)_3]$ end groups. In addition, a mononuclear model complex was prepared for comparison. All three manganese compounds are stable in solution and in the air for an extended period of time in the absence of light. However, upon photoactivation at 410 nm using a custom-made LED light source, CO-release studies with the myoglobin assay showed that at least two of the three carbonyl ligands per $Mn(CO)_3$ moiety can be liberated under these conditions. The half-life and quantum yield of CO release were also similar for the first- and second-generation metallodendrimers, indicating that no scaling effects are operative in these systems and that each $[MnBr(bpy)(CO)_3]$ end group behaves independently from the others. The total amount of CO-released per molecular unit, on the other hand, of course increases with the dendrimer generation, reaching a value of 15 CO per molecule of the second-generation metallodendrimer. In addition, the electronic structure and main transitions thought to be involved in the photoinduced CO release have been studied for the model compound using DFT/TDDFT. In summary, we have successfully attached an increasing number of CORM groups to dendrimer carrier molecules and will now further investigate their biological activity in cellular systems.

ASSOCIATED CONTENT

Supporting Information

^1H NMR (6 figures), 2D-COSY NMR (1 figure), $^{13}C\{^1H\}$-NMR (3 figures) and HR-ESI-TOF (2 figures) spectra of ligands and complexes, IR spectra showing decrease of the metal−carbonyl bands for **2** and **3** upon extended exposure to daylight (2 figures), UV/vis spectral traces showing dark stability and photolysis of **1**−**3** in dimethylsulfoxide/water solution (3 figures), change of absorption at selected wavelengths for dark stability and photolysis of 1−3 under the conditions of the myoglobin assay (3 figures), expanded dark stability experiments for **2** and **3** under the conditions of the myoglobin assay (2 figures), spectral changes in the Q-band region of myoglobin upon photoactivation of **2** and **3** (2 figures), formation of MbCO with increasing photoactivation time of **2** and **3** (2 figures). DFT-optimized geometries of **3-A** to **3-C** (1 figure and 3 tables) and comparison with published data (1 table). This material is available free of charge via the Internet at http://pubs.acs.org.

AUTHOR INFORMATION

Corresponding Author

*E-mail: ulrich.schatzschneider@uni-wuerzburg.de; gregory.smith@uct.ac.za.

Notes

The authors declare no competing financial interest.

ACKNOWLEDGMENTS

Financial support from the University of Cape Town (UCT), the National Research Foundation of South Africa (NRF), the South African Medical Research Council (MRC), the Deutscher Akademischer Austausch Dienst (DAAD), and the Bundesministerium für Bildung und Forschung (BMBF, project SUA 10/029) is gratefully acknowledged for several short term exchange visits between the two laboratories. Even though this work is supported by the MRC, the views and opinions expressed are not those of the MRC but of the authors of the material produced or publicized. We would like to thank Mr. Wolfgang Obert from the electronics workshop of the Institut für Anorganische Chemie of the Universität Würzburg for the expert construction of the LED setup.

REFERENCES

(1) Foresti, R.; Motterlini, R. *Curr. Drug Targets* **2010**, *11*, 1595−1604.
(2) Hou, Y. C.; Janczuk, A.; Wang, P. G. *Curr. Pharm. Des.* **1999**, *5*, 417−441.
(3) Li, L.; Rose, P.; Morre, P. K. *Annu. Rev. Pharmacol. Toxicol.* **2011**, *51*, 169−187.
(4) Matsui, T.; Furukawa, M.; Unno, M.; Tomita, T.; Ikeda-Saito, M. *J. Biol. Chem.* **2005**, *280*, 2981−2989.
(5) Motterlini, R.; Otterbein, R. M. *Nat. Rev. Drug Discovery* **2010**, *9*, 728−743.
(6) Motterlini, R.; Foresti, R.; Green, C. J. Studies on the development of carbon monoxide−releasing molecules: potential applications for the treatment of cardiovascular dysfunction. In *Carbon Monoxide and Cardiovascular Function*; Wang, R., Ed.; CRC Press: Boca Raton, FL, 2002; pp 249−271.
(7) Motterlini, R.; Clark, J. E.; Foresti, R.; Sarathchandra, P.; Mann, B. E.; Green, C. J. *Circ. Res.* **2002**, *90*, e17−e24.
(8) Clark, J. E.; Naughton, P.; Shurey, S.; Green, C. J.; Johnson, T. R.; Mann, B. E.; Foresti, R.; Motterlini, R. *Circ. Res.* **2003**, *93*, e2−e8.
(9) Johnson, T. R.; Mann, B. E.; Teasdale, I. P.; Adams, H.; Foresti, R.; Green, C. J.; Motterlini, R. *Dalton Trans.* **2007**, 1500−1508.
(10) Mann, B. E. *Top. Organomet. Chem.* **2010**, *32*, 247−285.
(11) Mann, B. E. *Organometallics* **2012**, *31*, 5728−5735.
(12) Bikiel, D. E.; Gonzalez Solveyra, E.; Milagre, H.; Eberlin, M.; Estrin, D. A.; Doctorovich, F. *Inorg. Chem.* **2011**, *50*, 2334−2345.
(13) Zobi, F.; Degonda, A.; Schaub, M. C.; Bogdanova, A. Y. *Inorg. Chem.* **2010**, *49*, 7313−7322.
(14) Zobi, F.; Blacque, O.; Jacobs, R. A.; Schaub, M. C.; Bogdanova, A. Y. *Dalton Trans.* **2012**, *41*, 370−378.
(15) Zobi, F.; Blacque, O. *Dalton Trans.* **2011**, *40*, 4994−5001.
(16) Fairlamb, I. J. S.; Duhme-Klair, A.-K.; Lynam, J. M.; Moulton, B. E.; O' Brien, C. T.; Sawle, P.; Hammad, J.; Motterlini, R. *Bioorg. Med. Chem. Lett.* **2006**, *16*, 995−998.
(17) Fairlamb, I. J. S.; Lynam, J. M.; Moulton, B. E.; Taylor, I. E.; Duhme-Klair, A.-K.; Sawle, P.; Motterlini, R. *Dalton Trans.* **2007**, 3603−3605.
(18) Romão, C. C.; Blättler, W. A.; Seixas, J. D.; Bernardes, G. J. L. *Chem. Soc. Rev.* **2012**, *41*, 3571−3583.
(19) Romanski, S.; Kraus, B.; Schatzschneider, U.; Neudörfl, J.-M.; Amslinger, S.; Schmalz, H.-G. *Angew. Chem., Int. Ed.* **2011**, *50*, 2392−2396.
(20) Romanski, S.; Kraus, B.; Guttentag, M.; Schlundt, W.; Rücker, H.; Adler, A.; Neudörfl, J.-M.; Alberto, R.; Amslinger, S.; Schmalz, H.-G. *Dalton Trans.* **2012**, *41*, 13862−13875.
(21) Romanski, S.; Rücker, H.; Stamellou, E.; Guttentag, M.; Neudörfl, J.-M.; Alberto, R.; Amslinger, S.; Yard, B.; Schmalz, H.-G. *Organometallics* **2012**, *31*, 5800−5809.
(22) Schatzschneider, U. *Inorg. Chim. Acta* **2011**, *374*, 19−23.
(23) Alberto, R.; Motterlini, R. *Dalton Trans.* **2007**, *17*, 1651−1660.
(24) Rimmer, R. D.; Richter, H.; Ford, P. C. *Inorg. Chem.* **2010**, *49*, 1180−1185.

(25) Rimmer, R. D.; Pierri, A. E.; Ford, P. C. *Coord. Chem. Rev.* **2012**, *256*, 1509−1519.
(26) Pierri, A. E.; Pallaoro, A.; Wu, G.; Ford, P. C. *J. Am. Chem. Soc.* **2012**, *134*, 18197−18200.
(27) Yu, H.; Li, J.; Wu, D.; Qiu, Z.; Zhang, Y. *Chem. Soc. Rev.* **2010**, *39*, 464−473.
(28) Klan, P.; Solomek, T.; Bochet, C. G.; Blanc, A.; Givens, R.; Rubina, M.; Popik, V.; Kostikov, A.; Wirz, J. *Chem. Rev.* **2013**, *113*, 119−191.
(29) Schatzschneider, U. *Eur. J. Inorg. Chem.* **2010**, 1451−1467.
(30) Brown, S. B.; Brown, E. A.; Walker, I. *Lancet Oncol.* **2004**, *5*, 497−508.
(31) Zhang, W.-Q.; Atkin, A. J.; Fairlamb, I. J. S.; Whitwood, A. C.; Lynam, J. M. *Organometallics* **2011**, *30*, 4643−4654.
(32) Niesel, J.; Pinto, A.; Peindy N'Dongo, H. W.; Merz, K.; Ott, I.; Gust, R.; Schatzschneider, U. *Chem. Commun.* **2008**, 1798−1800.
(33) Pfeiffer, H.; Rojas, A.; Niesel, J.; Schatzschneider, U. *Dalton Trans.* **2009**, 4292−4298.
(34) Dördelmann, G.; Pfeiffer, H.; Birkner, A.; Schatzschneider, U. *Inorg. Chem.* **2011**, *50*, 4362−4367.
(35) Dördelmann, G.; Meinhardt, T.; Sowik, T.; Krüger, A.; Schatzschneider, U. *Chem. Commun.* **2012**, *48*, 11528−11530.
(36) Brückmann, N. E.; Wahl, M.; Reiß, G. J.; Kohns, M.; Wätjen, W.; Kunz, P. C. *Eur. J. Inorg. Chem.* **2011**, 4571−4577.
(37) Peer, D.; Karp, J. M.; Hong, S.; Farokhzad, O. C.; Margalit, R.; Langer, R. *Nat. Nanotechnol.* **2007**, *2*, 751−760.
(38) Astruc, D. *Pure Appl. Chem.* **2003**, *75*, 461−481.
(39) Hwang, S.-H.; Shreiner, C. D.; Moorefield, C. N.; Newkome, G. R. *New J. Chem.* **2007**, *31*, 1192−1217.
(40) Govender, P.; Therrien, B.; Smith, G. S. *Eur. J. Inorg. Chem.* **2012**, 2853−2862.
(41) El Kazzouli, S.; El Brahmi, N.; Mignani, S.; Bousmina, M.; Zablocka, M.; Majoral, J.-P. *Curr. Med. Chem.* **2012**, *19*, 4995−5010.
(42) Govender, P.; Renfrew, A. K.; Clavel, C. M.; Dyson, P. J.; Therrien, B.; Smith, G. S. *Dalton Trans.* **2011**, *40*, 1158−1167.
(43) Govender, P.; Antonels, N. C.; Mattsson, J.; Renfrew, A. K.; Dyson, P. J.; Moss, J. R.; Therrien, B.; Smith, G. S. *J. Organomet. Chem.* **2009**, *694*, 3470−3476.
(44) Govender, P.; Sudding, L. C.; Clavel, C. M.; Dyson, P. J.; Therrien, B.; Smith, G. S. *Dalton Trans.* **2013**, *42*, 1267−1277.
(45) Payne, R.; Govender, P.; Therrien, B.; Clavel, C. M.; Dyson, P. J.; Smith, G. S. *J. Organomet. Chem.* **2013**, *729*, 20−27.
(46) Atkin, A. J.; Lynam, J. M.; Moulton, B. E.; Sawle, P.; Motterlini, R.; Boyle, N. M.; Pryce, M. T.; Fairlamb, I. J. S. *Dalton Trans.* **2011**, *40*, 5755−5761.
(47) McLean, S.; Mann, B. E.; Poole, R. K. *Anal. Biochem.* **2012**, *427*, 36−40.
(48) Ward, J. S.; Lynam, J. M.; Moir, J. W. B.; Sanin, D. E.; Mountford, A. P.; Fairlamb, I. J. S. *Dalton Trans.* **2012**, *41*, 10514−10517.
(49) Gonzalez, M. A.; Yim, M. A.; Cheng, S.; Moyes, A.; Hobbs, A. J.; Mascharak, P. K. *Inorg. Chem.* **2012**, *51*, 601−608.
(50) Kunz, P. C.; Huber, W.; Rojas, A.; Schatzschneider, U.; Spingler, B. *Eur. J. Inorg. Chem.* **2009**, 5358−5366.
(51) Szacilowski, K.; Macyk, W.; Drzewiecka-Matuszek, A.; Brindell, M.; Stochel, G. *Chem. Rev.* **2005**, *105*, 2647−2694.
(52) Antonini, E.; Brunori, M. In *Frontiers of Biology*; Neuberger, A., Tatum, E. L., Eds.; North-Holland: Amsterdam, 1971; p 19.
(53) Crook, S. H.; Mann, B. E.; Meijer, A. J. H. M.; Adams, H.; Sawle, P.; Scapens, D.; Motterlini, R. *Dalton Trans.* **2011**, *40*, 4230−4235.
(54) Mohr, F.; Niesel, J.; Schatzschneider, U.; Lehmann, C. W. *Z. Anorg. Allg. Chem.* **2012**, *638*, 543−546.
(55) Jackson, C. S.; Schmitt, S.; Ping Dou, Q.; Kodanko, J. J. *Inorg. Chem.* **2011**, *50*, 5336−5338.
(56) Hatchard, C. G.; Parker, C. A. *Proc. R. Soc. London, Ser. A* **1956**, *235*, 518−536.
(57) Parker, C. A. *Proc. R. Soc. London, Ser. A* **1953**, *220*, 104−116.
(58) Wieland, S.; van Eldik, R. *J. Phys. Chem.* **1990**, *94*, 5865−5870.
(59) Horn, E.; Snow, M. R.; Tiekink, E. R. T. *Acta Crystallogr.* **1987**, *C43*, 792−794.
(60) Stor, G. J.; Stufkens, D. J.; Vernooijs, P.; Baerends, E. J.; Fraanje, J.; Goubitz, K. *Inorg. Chem.* **1995**, *34*, 1588−1594.
(61) Rauhut, G.; Pulay, P. *J. Phys. Chem.* **1995**, *99*, 3093−3100.
(62) Wong, M. W. *Chem. Phys. Lett.* **1996**, *256*, 391−399.
(63) Neese, F. *Coord. Chem. Rev.* **2009**, *253*, 526−563.
(64) Gonzalez, M. A.; Carrington, S. J.; Fry, N. L.; Martinez, J. L.; Mascharak, P. K. *Inorg. Chem.* **2012**, *51*, 11930−11940.
(65) Peek, B. M.; Ross, G. T.; Edwards, S. W.; Meyer, G. J.; Meyer, T. J.; Erickson, B. W. *Int. J. Peptide Protein Res.* **1991**, *38*, 114−123.
(66) Busche, C.; Comba, P.; Mayboroda, A.; Wadepohl, H. *Eur. J. Inorg. Chem.* **2010**, 1295−1302.
(67) Fulmer, G. R.; Miller, A. J. M.; Sherden, N. H.; Gottlieb, H. E.; Nudelman, A.; Stoltz, B. M.; Bercaw, J. E.; Goldberg, K. I. *Organometallics* **2010**, *29*, 2176−2179.
(68) Kuhn, H. J.; Braslavsky, S. E.; Schmidt, R. *Pure Appl. Chem.* **1989**, *61*, 187−210.
(69) Neese, F. *WIREs Comput. Mol. Sci.* **2011**, *2*, 73−78.
(70) Schaefer, A.; Horn, H.; Ahlrichs, R. *J. Chem. Phys.* **1992**, *97*, 2571−2577.
(71) Weigend, F.; Ahlrichs, R. *Phys. Chem. Chem. Phys.* **2005**, *7*, 3297−3305.